A strange star scenario for the formation of eccentric millisecond pulsar PSR J1946+3417

Long Jiang[1,2,3], Na Wang[1], Wen-Cong Chen[2,3], Wei-Min Liu[3], Chun-Wei Leng[3], Jian-Ping Yuan[1] and Xiang-Li Qian[4]

[1] Xinjiang Astronomical Observatory, Chinese Academy of Sciences, Urumqi 830011, China; *na.wang@xao.ac.cn*
[2] School of Science, Qingdao University of Technology, Qingdao 266525, China; *chenwc@pku.edu.cn*
[3] School of Physics and Electrical Information, Shangqiu Normal University, Shangqiu 476000, China
[4] Department of Intelligent Engineering, Shandong Management University, Jinan 250357, China

Abstract PSR J1946 + 3417 is a millisecond pulsar (MSP) with a spin period $P \simeq 3.17\,\mathrm{ms}$. Harbored in a binary with an orbital period $P_{\mathrm{b}} \simeq 27$ days, the MSP is accompanied by a white dwarf (WD). The masses of the MSP and the WD were determined to be $1.83\,M_\odot$ and $0.266\,M_\odot$, respectively. Specially, its orbital eccentricity is $e \simeq 0.134$, which is challenging the recycling model of MSPs. Assuming that the neutron star in a binary may collapse to a strange star when its mass reaches a critical limit, we propose a phase transition (PT) scenario to account for the origin of the system. The sudden mass loss and the kick induced by asymmetric collapse during the PT may result in the orbital eccentricity. If the PT event takes place after the mass transfer ceases, the eccentric orbit cannot be re-circularized in the Hubble time. Aiming at the masses of both components, we simulate the evolution of the progenitor of PSR J1946 + 3417 via MESA. The simulations show that an NS / main sequence star binary with initial masses of $1.4 + 1.6\,M_\odot$ in an initial orbit of 2.59 days will evolve into a binary consisting of a $2.0\,M_\odot$ MSP and a $0.27\,M_\odot$ WD in an orbit of ~ 21.5 days. Assuming that the gravitational mass loss fraction during PT is 10%, we simulate the effect of PT via the kick program of BSE with a velocity of $\sigma_{\mathrm{PT}} = 60\,\mathrm{km\,s^{-1}}$. The results show that the PT scenario can reproduce the observed orbital period and eccentricity with higher probability than other values.

Key words: stars: neutron — stars: evolution — pulsars: individual (J1946+3417)

1 INTRODUCTION

Pulsars with weak surface magnetic fields ($B \simeq 10^8 - 10^9\,\mathrm{G}$) and short spin periods ($P \leq 20\,\mathrm{ms}$) are known as millisecond pulsars (MSPs). They are neutron stars (NSs) which were spun up to millisecond period in low-mass X-ray binaries (LMXBs) by the accretion of mass and angular momentum (Manchester 2004; Lorimer 2008). This is the widely accepted standard recycling model (Alpar et al. 1982; Radhakrishnan & Srinivasan 1982; Bhattacharya & van den Heuvel 1991). Harbored in pre-LMXBs with initial orbital periods longer than the so-called bifurcation period (Pylyser & Savonije 1989), the donor stars always lose their hydrogen envelopes and evolve into He white dwarfs (WDs). Considering the tidal interaction with a long timescale during the mass transfer, MSPs are expected to be found in binaries with circularized-orbits (Phinney 1992) unless they have ever experienced some dynamical

processes in dense globular clusters (Verbunt et al. 1987; Verbunt 1988).

The discovery of several eccentric MSP (eMSP) binaries presented a challenge to the recycling model. PSR J1903+0327 (hereafter J1903) is the first reported eMSP located in the Galactic field. Accompanied by a G-type main sequence (MS) star, the eccentricity of this source is $e \simeq 0.44$ (Champion et al. 2008). Liu & Li (2009) suggested that it is a newborn NS which is experiencing an accretion from the supernova fallback disk, while another evolutionary channel suggests that it originates from a hierarchical triple system (Freire et al. 2011; Portegies Zwart et al. 2011; Pijloo et al. 2012). PSR J1618−3921 (hereafter J1618) is the second reported Galactic field eMSP with $e \simeq 0.027$ (Bailes 2010). Its spin period is $P \simeq 12\,\mathrm{ms}$, and the orbital period is $P_{\mathrm{b}} \simeq 22.7$ days. According to its mass function, the companion star should be a He WD (Octau et al. 2018).

Subsequently, four Galactic field eMSPs with similar orbital properties have been discovered. They are PSRs J2234+0611 (hereafter J2234, Deneva et al. 2013), J1946+3417 (hereafter J1946, Barr et al. 2013), J1950+2414 (hereafter J1950, Knispel et al. 2015), and J0955−6150 (hereafter J0955, Camilo et al. 2015). As listed in Table 1, they share some similar properties, i.e., (1) orbital eccentricities vary from 0.08 to 0.14, (2) accompanied by He WDs with masses from 0.2 to 0.3 $M_\odot$, (3) orbital periods lie in the range from 22 to 32 days, (4) their short spin periods ($P \leq 5.0$ ms) which indicate long-lasting mass transfer episodes during their LMXB phase. Their strong similarities are not expected to result from the disruption of triple systems like J1903, since such a chaotic process should produce a wide range of orbital eccentricities and orbital periods.

At present, three evolutionary channels forming eMSPs were proposed. First, the accretion-induced collapse (AIC, Nomoto et al. 1979; Miyaji et al. 1980; Taam & van den Heuvel 1986; Canal et al. 1990; Nomoto & Kondo 1991) of massive ONe WDs may produce MSPs (for review, see Wang & Liu 2020). Freire & Tauris (2014) suggested that these eMSPs were formed by the rotation delayed AIC (RD-AIC) of massive ONe WDs with masses of $\sim 1.2\,M_\odot$. In a binary consisting of a massive ONe WD and an MS companion, the evolving MS star will transfer hydrogen-rich material onto the WD when it overflows its Roche lobe. For a rapidly rotating WD, its mass can exceed the Chandrasekhar limit without collapsing to an NS (Yoon & Langer 2004). When the mass transfer ceased, the WD will spin-down. If the centrifugal forces cannot sustain the hydrostatic equilibrium, the WD will collapse. The sudden released gravitational binding energy during the collapse will imposes eccentricity on the circular orbit. Since the re-circularization timescale are generally much longer than the Hubble time (Zahn 1977; Hut 1981), such MSP/He WD binaries will be eMSP binaries. Second, Antoniadis (2014) proposed a circumbinary (CB) disk scenario. He suggested that the dynamical interaction between the binary and a CB disk may cause the eccentricity. In this scenario, the CB disk originates from the escaping material from the donor star during hydrogen-shell flash shortly before the WD cooling phase. Adopting the linear perturbation theory given by Dermine et al. (2013), his calculation show that a CB disk with a fine-tuned lifetime as long as $\sim 10^5$ years and a mass around $\sim 10^{-4}\,M_\odot$ could result in an eccentricity of $0.01 \leq e \leq 0.15$ for post-LMXBs with orbital periods between 15 and 50 days. Third, considering that phase transition (PT) from NSs to strange stars (SSs) may occur when the core density of accreting NSs in LMXBs reaches the critical density for quark de-confinement, Jiang et al. (2015) (hereafter Paper 1) argued the NS-SS PT scenario. Similar to the RD-AIC model, the calculation in Paper 1

shows that the sudden gravitational mass loss of the NS during PT can produce the observed eccentricities.

Recently, accurate mass measurements of some eMSPs were reported, which may provide some clues on their formation channel. As shown in Table 1, the measurement of J2234 yields $M_1 \simeq 1.35\,M_\odot$ for the MSP and $M_2 \simeq 0.30\,M_\odot$ for its companion (Stovall et al. 2019). Based on the timing observations of J1950 from the data of Arecibo ALFA pulsar survey, Zhu et al. (2019) derived $M_1 \simeq 1.50\,M_\odot$, and $M_2 \simeq 0.28\,M_\odot$ for the MSP and the WD, respectively. It seems that the mass measurements of both J1950 and J2234 prefer to the RD-AIC scenario. However, this scenario tends to produce a low-mass MSP. Even if the mass increase of WD due to differential rotation are considered, a specific accretion rate is also difficult to satisfy (Yoon & Langer 2004). Therefore, the RD-AIC scenario is difficult to account for the formation of J1946 with a high MSP mass ($M_1 \simeq 1.83\,M_\odot$) (Barr et al. 2017). Furthermore, CB disks surrounding the binary MSPs can result in the formation of eMSPs with high NS masses, whereas the hydrogen-shell flashes generally exist in the final evolutionary stages of LMXBs, which is contrary to the rarity of eMSPs in the binary MSPs population. As a peculiar eMSP, the formation of PSR J1946 is difficult to understand by the RD-AIC or CB disk scenario. Employing a detailed binary evolution model, in this work we attempt to diagnose whether the NS-SS PT scenario can be responsible for the formation of PSR J1946.

This paper is arranged as follows. The NS-SS PT scenario is discussed in Section 2, whereas the stellar evolution code and the spin evolution of NS are described in Section 3. The simulated results and the influence of PT kick on the evolution of post-LMXBs are presented in Sections 4 and 5, respectively. Finally, we give a brief summary in Section 6.

2 STRANGE STAR SCENARIO

Considering that the strange quark matter is most stable, the concept of SS was proposed (Itoh 1970; Bodmer 1971; Farhi & Jaffe 1984; Witten 1984; Alcock et al. 1986; Haensel et al. 1986; Xu 2003; Lai & Xu 2009; Liu et al. 2012), i.e., some pulsars may be SSs instead of NSs. Believing that both NSs and SSs coexist in the Universe, it was argued that NS-SS PT may occur when the central density of an NS rises above the quark de-confinement density (Berezhiani et al. 2003; Bombaci et al. 2004, 2008; Zhu et al. 2013; Bombaci et al. 2016; Drago et al. 2016; Bhattacharyya et al. 2017; Wiktorowicz et al. 2017; Hou et al. 2018; Alvarez-Castillo et al. 2019).

Studying the equation of state (EoS) of neutron-rich matter, Staff et al. (2006) propose that the critical density for quark de-confinement is about five times of the nuclear saturation density. For a rapidly spinning NS,

Table 1 Some Observed Parameters of Six Known Galactic Field eMSPs

PSR	P (ms)	$\dot{P}$ (s s^{-1})	$P_{\rm b}$ (days)	e	M_1 ($M_\odot$)	M_2 ($M_\odot$)	Companion type	τ (Gyr)*	Ref.
J1903	2.15	1.88×10^{-20}	95.2	0.437	-	1.08*	MS	1.81	Freire et al. (2011)
J1618	11.99	5.41×10^{-20}	22.7	0.027	-	0.20*	He WD	3.51	Bailes (2010)
J2234	3.58	1.2×10^{-20}	32.0	0.129	1.353	0.298	He WD	4.72	Stovall et al. (2019)
J1950	4.30	1.88×10^{-20}	22.2	0.080	1.496	0.28	He WD	3.63	Zhu et al. (2019)
J1946	3.17	3.12×10^{-21}	27.02	0.1345	1.828	0.2656	He WD	16.1	Barr et al. (2017)
J0955	2.00	−	24.6	0.11	-	≥ 0.21	He WD	-	Camilo et al. (2015)

Notes: $* \tau \equiv P/2\dot{P}$, the characteristic age; $\star$: No further measurement available, here is the median masses derived from the mass function assuming a random distribution of orbital inclinations and a pulsar mass of 1.35 $M_\odot$. See http://www.atnf.csiro.au/research/pulsar/psrcat, Manchester et al. (2005).

the centrifugal force might reduce the central density and increase the maximum mass. With spin period P, this can be expressed as (Hartle 1970; Baym et al. 1971):

$$M_c(P) = M_c(0) + \delta M(P_{\rm min}/P)^2, \qquad (1)$$

where $P_{\rm min}$ is the minimum spin period (in this work, we take $P_{\rm min} = 1$ ms), $M_c(0)$ is the maximum mass of the non-rotating NS, δM denotes the rotation induced maximum mass increase. Lasota et al. (1996) found that for a rigid rotating NS, $\delta M/M_c(0) \sim 20\%$ while Morrison et al. (2004) and Haensel et al. (2007) derived that this ratio is about 50% for a differentially rotating NS.

In current work, we take $M_c(0) = 1.8\,M_\odot$ (Akmal et al. 1998), and $\delta M = 0.4\ M_\odot$ (Lasota et al. 1996). The PT process is assumed to take place when the mass of the NS, $M_{\rm NS}$, exceeds its maximum mass at a spin period of P, $M_c(P)$. It can occur in the spin-up stage induced by the accretion, or in the spin-down stage of NS after the accretion ceased. The latter is defined as delayed PT, which can be applied to J1946.

In the recycling stage, the NS would be spun up by accreted material from the donor star. Cheng & Zhang (2000) derived an expression for the spin period evolution of the NS:

$$
P = \max\left[1.1\left(\frac{M_{\rm NS}-M_{\rm NS,i}}{M_\odot}\right)^{-1} R_6^{-5/14}\right.
$$
$$
\times I_{45}\left(\frac{M_{\rm NS}}{M_\odot}\right)^{-1/2}, \qquad (2)
$$
$$
\left.1.1\left(\frac{M_{\rm NS}}{M_\odot}\right)^{-1/2} R_6^{17/14}\right] \text{ ms},
$$

where R_6 is the radius of the NS in units of 10^6 cm, I_{45} is the moment of inertia of the NS in units of 10^{45} g cm^2, ($R_6 = I_{45} = 1$ in this work), and $M_{\rm NS,i}$ is the initial mass of the NS.

The difference between the gravitational masses of NS and SS with the same baryon number is also widely studied (Bombaci & Datta 2000; Drago et al. 2007; Marquez & Menezes 2017). It is generally thought $\Delta M = M_{\rm NS} - M_{\rm SS} \approx 0.15\ M_\odot$ for NS with a mass of $M_{\rm NS} \simeq 1.5\ M_\odot$[1],

i.e., the mass loss ratio $\Delta M/M_{\rm NS}$ during PT is about 10%. Following their researches, in this work, we take the mass of SS $M_{\rm SS} = 0.9 M_{\rm NS}$. Assuming J1946 is an SS formed via NS-SS PT, the mass of the NS before PT can be derived to be $2.00-2.06\ M_\odot$ according to the current mass $M_{\rm SS} = 1.828(22)\ M_\odot$ (Barr et al. 2017).

The detailed PT process from baryons to quarks is not well understood. Olinto (1987) and Horvath & Benvenuto (1988) believed that the PT will last around 10^8 yr as a gradual process, while many researchers argued that the process might be a detonation mode with timescale from several milliseconds to ~ 10 seconds (Cheng & Dai 1996; Ouyed et al. 2002; Shu et al. 2017; Prasad & Mallick 2018; Zhang et al. 2018; Mariani et al. 2019; Ouyed et al. 2013, 2020; Mallick et al. 2020). Their studies show that the energy released during PT is compatible with a core collapse supernova (CCSN). We consider that the PT takes place in the core of NS like CCSN, and a kick velocity V_k is imparted to the new born SS due to a spherical asymmetric collapse[2]. Since the mass transfer timescale is of order of 10^8yr, the binary orbit before PT is assumed to be circular. Setting the positional angle of V_k with respect to the pre-PT orbital plane as ϕ, and the angle between V_k and the pre-PT orbital velocity V_0 as θ, then the ratio between the semi-major axes before and after PT is (Hills 1983; Dewi & Pols 2003; Shao & Li 2016)

$$\frac{a_0}{a} = 2 - \frac{M_T}{M_T - \Delta M}(1+\nu+2\nu\cos\theta), \qquad (3)$$

where $\nu = V_k/V_0$, $V_0 = (2\pi G M_T/P_{\rm b,0})^{1/3}$, $P_{\rm b,0}$ and M_T are the orbital period and the total mass of the binary before PT, respectively. Because of the influence of sudden mass loss and the kick, the eccentricity after PT satisfies (Hills 1983; Dewi & Pols 2003; Shao & Li 2016)

$$
e^2 = 1 - \frac{a_0 M_T}{a(M_T - \Delta M)}\left[1 + 2\nu\cos\theta\right.
$$
$$
\left. + \nu^2(\cos^2\theta + \sin^2\theta\sin^2\phi)\right]. \qquad (4)
$$

The kick velocity distribution during PT is described as a Maxwellian distribution with one-dimensional rms

---

[1] A lower value may also be possible. For instance, Schaffner-Bielich et al. (2002) suggest that the difference of the gravitational masses between NS and hyperon star is $\simeq 0.03\ M_\odot$.

[2] The disruption of spherical symmetry might originate from the fast rotation of NSs or the dipole magnetic field. However, the detailed process is currently poorly understood.
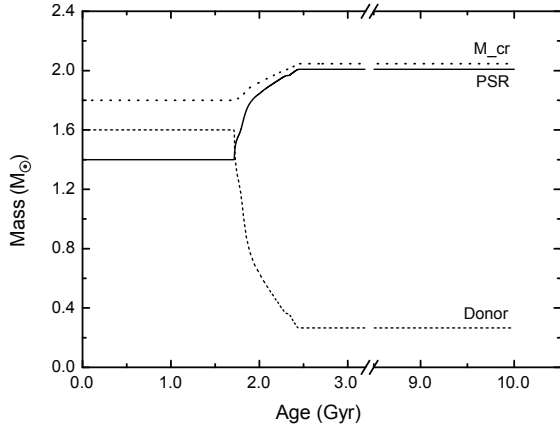
Fig. 1 Mass evolution of Model A. The *solid*, *dashed*, and *dotted curves* represent the NS mass, the donor star mass, and the critical mass, respectively. Since the mass of the NS is always lower than its critical mass, the PT process is delayed to the spin-down stage after RLOF ceases.

Fig. 2 Orbital period evolution of Model A.

σ_{PT}. By analysing the proper motions of 233 pulsars Hobbs et al. (2005) obtained a mean speed of $54(6)\mathrm{kms}^{-1}$ for recycled pulsars. Employing the rapid binary population synthesis (BPS) code (Hurley et al. 2000, 2002) and a weak kick velocity of $\sigma_{\mathrm{PT}} = 60$ km s^{-1}, Jiang et al. (2020) (hereafter Paper 2) studied the formation of isolated MSPs via NS-SS PT (a similar work is performed by Nurmamat et al. 2019). Paper 2 shows that, almost all the PT processes take place at the Roche Lobe overflow (RLOF) stage. However, it is also possible to take place after mass transfer ceases, and induce the formation of eccentric binary MSPs like J1946.

3 SIMULATION DESCRIPTION

3.1 Binary Evolution

To obtain the orbital properties of J1946 before PT, we simulated the evolution of its progenitor via MESAbinary in MESA (version r − 9575) (Paxton et al. 2011, 2013, 2015). The starting point of the simulation is a circular binary system containing a primary NS and a zero-age MS companion star with a solar composition ($X = 0.70$, $Y = 0.28$ and $Z = 0.02$).

During the mass transfer, we adopt the accretion efficiency $f = 1 - \alpha - \beta - \delta$ described by Tauris & van der Klis (2006), where α and β are the fraction of mass lost from the vicinity of the donor and the NS, respectively, while δ is the fraction of mass lost as coplanar toroid circling the binary. In current work, $\alpha = \delta = 0$ is adopted. In addition, a fixed Eddington accretion rate of the NS, $\dot{M}_{\mathrm{Edd}} = 1.8 \times 10^{-8} M_\odot \, \mathrm{yr}^{-1}$, is also considered, i.e., $\dot{M}_{\mathrm{NS}} = \min(-f\dot{M}_{\mathrm{d}}, \dot{M}_{\mathrm{Edd}})$, which may cause some more mass loss from the vicinity of the NS. Besides the angular momentum loss due to mass loss as fast winds (Paxton et al. 2015; Deng et al. 2021), effects of gravitational
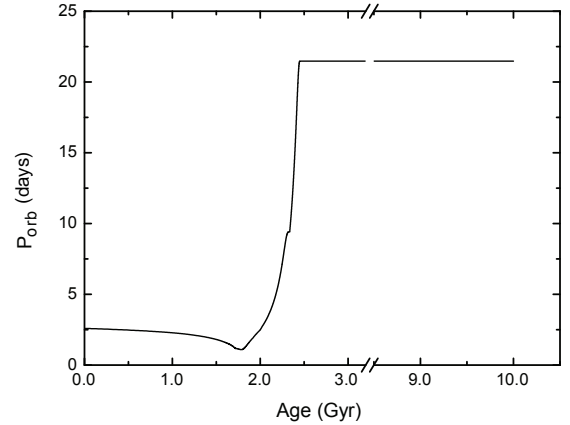
radiation (Landau & Lifshit's 1959; Faulkner 1971) and magnetic braking (with $\gamma = 3.0$, Rappaport et al. 1983; Paxton et al. 2015; Deng et al. 2020) are also considered.

3.2 Spin Evolution

For a delayed PT pulsar, its spin evolution can be divided into three stages. The first one is the spin-up process (see also Eq. (2)) during the recycling stage. The second one is the spin-down stage from the endpoint of RLOF (the stellar age is t_1) to the beginning of the NS-SS PT, in which the timescale is denoted by t_2 (it is also defined as the delay time). The third stage is the spin-down stage after PT (as an SS), denoting with a timescale t_3. Due to the uncertainties of EOS, the changes of spin period and magnetic field caused by PT are ignored.

The MSP is assumed to spin down according to a power law (Lyne et al. 1975), i.e., the spin period derivative $\dot{P} = KP^{(2-n)}$, where n is the braking index, and K is always a constant (indeed, it may also vary due to the evolution of magnetic field (Lyne et al. 1975)). Taking $R_6 = I_{45} = 1$, pure magnetic dipole radiation model ($n = 3$) with the magnetic inclination angle $\chi = 90°$ predicts a spin period derivative of the MSP as follows

$$\dot{P} = 0.98 \times 10^{-20} P_{\mathrm{ms}}^{-1} B_8^2 \text{ s s}^{-1}, \quad (5)$$

where P_{ms} is the spin period in units of 1 ms, B_8 is the surface magnetic field in units of 10^8 G (Woan et al. 2018).

Considering both the effect of residual field (Ding et al. 1993), and long term exponential decay (Urpin et al. 1994; Guseinov et al. 2004) with $t_{\mathrm{D}} = 10^8$ yr (Bransgrove et al. 2018; Xie & Zhang 2019)[3], we assume

$$B = \max\big[B_0\exp(-t/t_{\mathrm{D}}), \, B_{\min}\big], \quad (6)$$

where B_0 and $B_{\min}$ are the initial value and the minimum of surface magnetic field, respectively. In this work, we

---

[3] Smaller or larger values are also derived, for example, 3×10^6 yr (Guseinov et al. 2004), and 1.8×10^9 yr (Bransgrove et al. 2018). See Sun & Han (2002); Ruderman (2010), for review.
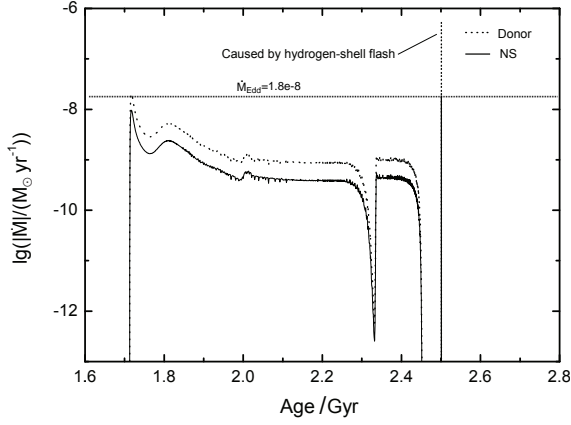
Fig. 3 Evolution of the mass transfer rates. *Dotted curve*: the donor star. *Solid curve*: the NS.

adopt a typical initial magnetic field of MSPs $B_0 = 10^9$ G, and $B_{\min} = 10^8$ G following Ding et al. (1993), which is similar to the current value 1.01×10^8 G of J1946 (Barr et al. 2017).

4 SIMULATED RESULTS

4.1 An evolutionary Example

With initial parameters, NS mass $M_{\mathrm{NS,i}} = 1.4 \, M_\odot$, companion mass $M_{\mathrm{d,i}} = 1.6 \, M_\odot$, orbital period $P_{\mathrm{b,i}} = 2.59 \, \mathrm{days}$, and $\beta = 0.5$ (which yields an accretion efficiency of 0.5, Podsiadlowski et al. 2002), we evolve Model A as a typical example. The masses evolutions of both the NS and the donor star are illustrated in Figure 1. The critical mass $M_c(P)$ of NS-SS PT is denoted by the dashed curve. It is clear that the NS mass is always lower than the critical mass during the mass transfer. This implies that the PT event will be delayed to the spin-down stage of the NS after the mass transfer ceases. Since the mass transfer timescale is as long as ~ 0.7 Gyr, the binary orbit will be circularized during RLOF, and keep circular until the PT takes place. As a result, for NSs without PT, the binary MSPs will be observed in circular orbit.

Figure 2 plots the orbital period evolution of Model A. Before the mass transfer or in the initial stage of the mass transfer, the orbit of pre-LMXB slowly shrinks in a timescale of ~ 1.8 Gyr due to the angular momentum loss driven by the magnetic braking. During the mass transfer ($\sim 1.8 - 2.5$ Gyr), the orbital period of LMXB gradually increase because the mass is transferring from the light donor star to the massive NS. After RLOF ceases (at the stellar age $t_1 \sim 2.5$ Gyr), the orbital period is approximately constant since the angular momentum loss induced by gravitational wave radiation in such a wide binary is very weak.

Figure 3 illustrates the evolution of the mass transfer rates. Since the material is transferring from the massive donor star to the light NS, mass transfer occurs on the
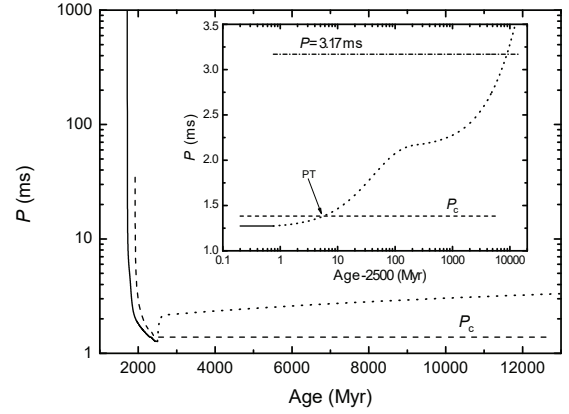

Fig. 4 Evolution of spin period of Model A. The *solid*, and *dotted curves* represent the spin-up (during RLOF) and the spin-down (mass transfer ceased) stages, respectively. The *dashed curve* denotes the evolution of critical period. In the insert panel, the cross point between the *dashed* and the *dotted curves* corresponds to the moment that the PT takes place, and the *dashed-dotted line* indicates the current spin period of J1946.

thermal timescale with a high rate ($\sim 10^{-8} \, M_\odot \, \mathrm{yr}^{-1}$). Once the mass ratio is below 1, the mass-transfer rate will decreases to $\sim 10^{-9} \, M_\odot \, \mathrm{yr}^{-1}$ sharply. The narrow single peak at the stellar age of ~ 2.5 Gyr is caused by the hydrogen-shell flash while the upper edge of the solid line in it reached the Eddington accretion rate. Since the flash may occur in most LMXB evolutions, formation of the CB disk and its effect (which is not considered in the current work) requires more study.

Spin period evolution of Model A is illustrated in Figure 4. The solid and dotted curves represent the spin-up and spin-down evolutionary stages, respectively. The dashed curve denotes the critical period that the PT occurs, which can be derived by $M_c(P) = M_{\mathrm{NS}}$ and Equation (1). In the insert panel, the cross point between the dashed and the dotted curves indicates the moment that the PT occur, which is at about 5 Myr (delay time, t_2) after the mass transfer ceases. Furthermore the total spin-down timescale is $t_2 + t_3 \sim t_3 \sim 9$ Gyr.

4.2 Selected Models

The input parameters and the simulated results of some models are summarized in Table 2. Their initial parameters, $M_{\mathrm{NS,i}}$, $M_{\mathrm{d,i}}$ and $P_{\mathrm{b,i}}$ are selected to evolve pre-LMXB to the progenitor of J1946 at the endpoint of RLOF, which is characterized by following points: (1) the final mass of the NS is $2.00 \, M_\odot \leq M_{\mathrm{NS,f}} \leq 2.06 \, M_\odot$; (2) the companion is a He WD with a mass of $0.2640 \leq M_{\mathrm{d,f}} \leq 0.2680 \, M_\odot$ (Barr et al. 2017). According to the relation between the WD mass and the orbital period (Tauris & Savonije 1999), all models predict a narrow final orbital period range: $20.8 \leq P_{\mathrm{b,f}} \leq 22.1$ days.

Table 2 Simulation for PSR J1946: Some Fine-tuned Examples

	Model A	Model B	Model C	Model D	J1946
β	0.5	0.5	0.3	0.5	-
$M_{\rm NS,i}$ ($M_\odot$)	1.40	1.35	1.40	1.60	-
$M_{\rm d,i}$ ($M_\odot$)	1.60	1.80	1.30	1.20	-
$P_{\rm b,i}$ (days)	2.59	2.46	2.87	2.77	-
$M_{\rm d,f}$ ($M_\odot$)	0.2651	0.2643	0.2651	0.2656	0.2656(19)
t_1 (Gyr)	2.5	1.7	4.6	6.3	-
$P_{\rm b,f}$ (days)	21.47	20.83	21.64	22.10	27.02
$L_{\rm WD}$ ($L_\odot/1000$)	0.23	0.16	0.67	1.15	-
$T_{\rm WD,eff}$ (1000K)	5.0	4.6	6.3	7.2	-
$M_{\rm NS,f}$ ($M_\odot$)	2.01	2.05	2.06	2.03	-
$M_{\rm c,f}$ ($M_\odot$)	2.05	2.13	2.10	1.93	-
Delayed PT	Yes	Yes	Yes	No	-
$M_{\rm SS}$ ($M_\odot$)	1.809	1.845	1.854	-	1.828(22)
P_0 (ms)	1.274	1.106	1.164	-	-
$P_{\rm c,f}$ (ms)	1.383	1.277	1.235	-	3.17
t_2 (Myr)	4.9	7.1	2.8	-	-
t_3 (Gyr)	8.9	9.5	9.3	-	-
t_T (Gyr)	11.4	11.2	13.9	-	-

As shown in Table 2, the NS is spun up to P_0 at the endpoint of RLOF. Inserting P_0 into Equation (1), one can derive the critical mass $M_{\rm c,f}$. Comparing with the final mass of the NS, we find that, similar to Model A, Models B and C are expected delayed PT models since $M_{\rm c,f} > M_{\rm NS,f}$. The PT will occur when the NSs spin down to the critical spin period, $P_{\rm c,f}$, which is derived by $M_{\rm c}(P) = M_{\rm NS,f}$ and Equation (1). For Model D, the NS-SS PT will take place during its RLOF stage. In the following evolution, the SS accretes a mass $\geq 0.1\,M_\odot$ in a timescale of $\geq 10^7$ yr and its orbit is re-circularized. Since delayed PT models are much rare (result of Paper 2), the results of NS-SS PT scenario are consistent with the observation that most MSPs are harbored in circular binaries.

For the PT delayed models, since the delay time, t_2, is only several Myr, the total spin-down time is $t_2 + t_3 \sim t_3 \sim 9$ Gyr. Furthermore, the total evolutionary time, $t_T = t_1 + t_2 + t_3$, of these models approximate to 11.4 Gyr except Model C. It seems that Model C should be ruled out since its total evolutionary timescale is slightly longer than the Hubble time (13.7 Gyr). However, a shorter spin-down timescale can be obtained with some fine-tuned period evolution parameters, e.g. a longer $t_{\rm D}$.

To compare with the observation, some observed parameters of J1946 are also listed in Table 2. It is worth noting that, since (1) the NS-SS PT process is not included in the MESA, and (2) $P_{\rm c,f}$ is the critical period that the PT occurs, $P_{\rm b,f}$ and $P_{\rm c,f}$ cannot be compared directly with the orbital period and spin period of J1946. In addition, the luminosities and effective temperatures of the WDs (at the stellar age about 13 Gyr) predicted by the MESA simulation are also given for further checking when more observations are available.
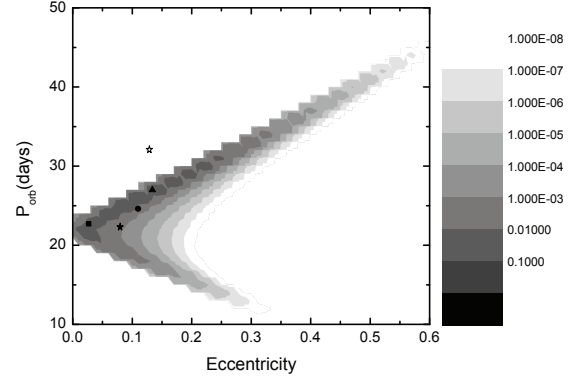
Fig. 5 Possibility distribution on the $P_{\rm b} - e$ diagram after PT kick. The *various level of gray* represents the possibility distribution. The *solid triangle*, *solid square*, *solid star*, *open star* and *circle* represent J1946, J1618, J1950, J2234, and J0955, respectively.

5 PT KICK

Taking the simulated results of MESA: $M_{\rm NS} = 2.03\,M_\odot$, $M_{\rm d} = 0.265\,M_\odot$ and $P_{\rm b} = 21.5$ days as input parameters before PT, we simulated the influence of PT on the post-LMXB by the subprogram kick.f of BPS developed by Hurley et al. (2000, 2002). A weak kick with velocity of $\sigma_{\rm PT} = 60$ km s^{-1} (Hobbs et al. 2005), and gravitational mass loss $\Delta M = 0.1 M_{\rm NS}$ during PT are adopted following Paper 2. The probability distribution of 10^{10} PT events in the $P_{\rm b} - e$ diagram is shown in Figure 4. The total probability that PT processes produce binary MSPs with $0.12 \leq e \leq 0.14$, and $26 \leq P_{\rm b} \leq 28$ is about 7.2%. Therefore, the NS-SS PT process is most likely evolutionary channel to J1946.

In Figure 5, the solid triangle, square, and circle correspond to J1946, J1618, and J0955, respectively. Although there is no further mass measurement of J1618 and J0955 except for the mass functions, the $P_{\rm b} - e$ diagram show that the NS-SS PT process may be responsible for the formation of these two sources. The another two eMSPs J1950 and J2234 are also shown as filled and open stars in the figure. However, their measured masses are too low to consistent with the NS-SS PT scenario.

Furthermore, the effects of PT on the post-LMXB include two respects. The first one is sudden mass loss, which results in an orbital expansion (the orbital period after PT is longer than before PT) and a constant eccentricity $e = \Delta M/M_{\rm T}$, as discussed in Paper 1. The second one is the kick (see also Eq. (4)), which results in spread distribution (alter the orbital period and eccentricity) as shown in Figure 5. The probability of PT producing orbital periods greater and less than 21.5 days are 88.6%, and 11.4%, respectively. In addition, the probability resulting in larger eccentricity ($e > 0.2$)

is relatively low ($\sim 15\%$). Obviously, a low or high kick velocity will result in a narrow or wide distribution range in the orbital period versus eccentricity diagram, respectively.

6 SUMMARY

In this work, we propose a delayed NS-SS PT scenario to account for the formation of eMSP J1946. Employing the stellar evolution code MESA, we simulated the evolution of its progenitor. The calculations indicate that a pre-LMXB consisting of an NS with an initial mass of $1.35 \leq M_{\rm NS,i} \leq 1.4\,M_\odot$ and an MS companion star (with a fine-tuning initial mass and an initial orbital period) can evolve into a post-LMXB consisting of a $\sim 2.0\,M_\odot$ NS and a $\sim 0.27\,M_\odot$ WD in an orbit of ~ 22 days. Because of a rapidly rotation, the NS would not collapse to SS during the RLOF. After the mass transfer ceases, NS-SS PT will take place when the NS spin down to a critical spin period $P_{\rm c,f}$.

Based on the simulated results of MESA, we study the influence of PT on the post-LMXB. A simulation of 10^{10} PT events is performed via the subprogram kick.f of BSE with a gravitational mass loss $\Delta M = 0.1\,M_{\rm NS}$, and weak kick $\sigma_{\rm PT} = 60$ km s^{-1}. The result shows that there are $\geq 7\%$ PT events producing $26 \leq P_{\rm b} \leq 28$ days and $0.12 \leq e \leq 0.14$, which are in good agreement with J1946. Our simulations also predict luminosities and effective temperatures of the WDs, which might be compared with and testified by future observations.

Additionally, the positions of J1618 and J0955 on the $P_{\rm b} - e$ diagram imply that they probably experienced evolutionary processes similar to J1946, which will be studied in detail when more mass information is available.

References

Akmal, A., Pandharipande, V. R., & Ravenhall, D. G. 1998, Phys. Rev. C, 58, 1804

Alcock, C., Farhi, E., & Olinto, A. 1986, ApJ, 310, 261

Alpar, M. A., Cheng, A. F., Ruderman, M. A., & Shaham, J. 1982, Nature, 300, 728

Alvarez-Castillo, D. E., Antoniadis, J., Ayriyan, A., et al. 2019, Astronomische Nachrichten, 340, 878

Antoniadis, J. 2014, ApJL, 797, L24

Bailes, M. 2010, New Astron. Rev., 54, 80

Barr, E. D., Freire, P. C. C., Kramer, M., et al. 2017, MNRAS, 465, 1711

Barr, E. D., Champion, D. J., Kramer, M., et al. 2013, MNRAS, 435, 2234

Baym, G., Pethick, C., & Sutherland, P. 1971, ApJ, 170, 299

Berezhiani, Z., Bombaci, I., Drago, A., et al. 2003, ApJ, 586, 1250

Bhattacharya, D., & van den Heuvel, E. P. J. 1991, Phys. Rep., 203, 1

Bhattacharyya, S., Bombaci, I., Logoteta, D., & Thampan, A. V. 2017, ApJ, 848, 65

Bodmer, A. R. 1971, Phys. Rev. D, 4, 1601

Bombaci, I., & Datta, B. 2000, ApJL, 530, L69

Bombaci, I., Logoteta, D., Vidaña, I., & Providência, C. 2016, European Physical Journal A, 52, 58

Bombaci, I., Panda, P. K., Providência, C., & Vidaña, I. 2008, Phys. Rev. D, 77, 083002

Bombaci, I., Parenti, I., & Vidaña, I. 2004, ApJ, 614, 314

Bransgrove, A., Levin, Y., & Beloborodov, A. 2018, MNRAS, 473, 2771

Camilo, F., Kerr, M., Ray, P. S., et al. 2015, ApJ, 810, 85

Canal, R., Garcia, D., Isern, J., & Labay, J. 1990, ApJL, 356, L51

Champion, D. J., Ransom, S. M., Lazarus, P., et al. 2008, Science, 320, 1309

Cheng, K. S., & Dai, Z. G. 1996, Phys. Rev. Lett., 77, 1210

Cheng, K. S., & Zhang, C. M. 2000, A&A, 361, 1001

Deneva, J. S., Stovall, K., McLaughlin, M. A., et al. 2013, ApJ, 775, 51

Deng, Z.-L., Gao, Z.-F., Li, X.-D., & Shao, Y. 2020, ApJ, 892, 4

Deng, Z.-L., Li, X.-D., Gao, Z.-F., & Shao, Y. 2021, ApJ, 909, 174

Dermine, T., Izzard, R. G., Jorissen, A., & Van Winckel, H. 2013, A&A, 551, A50

Dewi, J. D. M., & Pols, O. R. 2003, MNRAS, 344, 629

Ding, K. Y., Cheng, K. S., & Chau, H. F. 1993, ApJ, 408, 167

Drago, A., Lavagno, A., Pagliara, G., & Pigato, D. 2016, European Physical Journal A, 52, 40

Drago, A., Lavagno, A., & Parenti, I. 2007, ApJ, 659, 1519

Farhi, E., & Jaffe, R. L. 1984, Phys. Rev. D, 30, 2379

Faulkner, J. 1971, ApJL, 170, L99

Freire, P. C. C., & Tauris, T. M. 2014, MNRAS, 438, L86

Freire, P. C. C., Bassa, C. G., Wex, N., et al. 2011, MNRAS, 412, 2763

Guseinov, O. H., Ankay, A., & Tagieva, S. O. 2004, International Journal of Modern Physics D, 13, 1805

Haensel, P., Potekhin, A. Y., & Yakovlev, D. G. 2007, Neutron Stars 1 : Equation of State and Structure, 326 (New York:

Springer)

Haensel, P., Zdunik, J. L., & Schaefer, R. 1986, A&A, 160, 121

Hartle, J. B. 1970, ApJ, 161, 111

Hills, J. G. 1983, ApJ, 267, 322

Hobbs, G., Lorimer, D. R., Lyne, A. G., & Kramer, M. 2005, MNRAS, 360, 974

Horvath, J. E., & Benvenuto, O. G. 1988, Physics Letters B, 213, 516

Hou, S.-J., Liu, T., Xu, R.-X., et al. 2018, ApJ, 854, 104

Hurley, J. R., Pols, O. R., & Tout, C. A. 2000, MNRAS, 315, 543

Hurley, J. R., Tout, C. A., & Pols, O. R. 2002, MNRAS, 329, 897

Hut, P. 1981, A&A, 99, 126

Itoh, N. 1970, Progress of Theoretical Physics, 44, 291

Jiang, L., Li, X.-D., Dey, J., & Dey, M. 2015, ApJ, 807, 41

Jiang, L., Wang, N., Chen, W.-C., et al. 2020, A&A, 633, A45

Knispel, B., Lyne, A. G., Stappers, B. W., et al. 2015, ApJ, 806, 140

Lai, X. Y., & Xu, R. X. 2009, MNRAS, 398, L31

Landau, L. D., & Lifshit's, E. M. 1959, Theory of Elasticity (Pergamon Press; Reading, Mass., Addison-Wesley Pub. Co.)

Lasota, J.-P., Haensel, P., & Abramowicz, M. A. 1996, ApJ, 456, 300

Liu, X.-W., & Li, X.-D. 2009, ApJ, 692, 723

Liu, X. W., Liang, J. D., Xu, R. X., et al. 2012, MNRAS, 424, 2994

Lorimer, D. R. 2008, Living Reviews in Relativity, 11, 8

Lyne, A. G., Ritchings, R. T., & Smith, F. G. 1975, MNRAS, 171, 579

Mallick, R., Singh, S., & Prasad, R. 2021, MNRAS, 507, 1318

Manchester, R. N. 2004, Science, 304, 542

Manchester, R. N., Hobbs, G. B., Teoh, A., & Hobbs, M. 2005, AJ, 129, 1993

Mariani, M., Orsaria, M. G., Ranea-Sandoval, I. F., & Lugones, G. 2019, MNRAS, 489, 4261

Marquez, K. D., & Menezes, D. P. 2017, J. Cosmol. Astropart. Phys., 2017, 028

Miyaji, S., Nomoto, K., Yokoi, K., & Sugimoto, D. 1980, PASJ, 32, 303

Morrison, I. A., Baumgarte, T. W., & Shapiro, S. L. 2004, ApJ, 610, 941

Nomoto, K., & Kondo, Y. 1991, ApJL, 367, L19

Nomoto, K., Miyaji, S., Sugimoto, D., & Yokoi, K. 1979, in IAU Colloq. 53: White Dwarfs and Variable Degenerate Stars, eds. H. M. van Horn, V. Weidemann, & M. P. Savedoff, 56

Nurmamat, N., Zhu, C., Lü, G., et al. 2019, Journal of Astrophysics and Astronomy, 40, 32

Octau, F., Cognard, I., Guillemot, L., et al. 2018, A&A, 612, A78

Olinto, A. V. 1987, Physics Letters B, 192, 71

Ouyed, R., Dey, J., & Dey, M. 2002, A&A, 390, L39

Ouyed, R., Leahy, D., & Koning, N. 2020, RAA (Research in Astronomy and Astrophysics), 20, 027

Ouyed, R., Niebergal, B., & Jaikumar, P. 2012, Proceedings of CSQCD III conference, arXiv:1304.8048

Paxton, B., Bildsten, L., Dotter, A., et al. 2011, ApJS, 192, 3

Paxton, B., Cantiello, M., Arras, P., et al. 2013, ApJS, 208, 4

Paxton, B., Marchant, P., Schwab, J., et al. 2015, ApJS, 220, 15

Phinney, E. S. 1992, Philosophical Transactions of the Royal Society of London Series A, 341, 39

Pijloo, J. T., Caputo, D. P., & Portegies Zwart, S. F. 2012, MNRAS, 424, 2914

Podsiadlowski, P., Rappaport, S., & Pfahl, E. D. 2002, ApJ, 565, 1107

Portegies Zwart, S., van den Heuvel, E. P. J., van Leeuwen, J., & Nelemans, G. 2011, ApJ, 734, 55

Prasad, R., & Mallick, R. 2018, ApJ, 859, 57

Pylyser, E. H. P., & Savonije, G. J. 1989, A&A, 208, 52

Radhakrishnan, V., & Srinivasan, G. 1982, Current Science, 51, 1096

Rappaport, S., Verbunt, F., & Joss, P. C. 1983, ApJ, 275, 713

Ruderman, M. 2010, New Astron. Rev., 54, 110

Schaffner-Bielich, J., Hanauske, M., Stöcker, H., & Greiner, W. 2002, Phys. Rev. Lett., 89, 171101

Shao, Y., & Li, X.-D. 2016, ApJ, 816, 45

Shu, X.-Y., Huang, Y.-F., & Zong, H.-S. 2017, Modern Physics Letters A, 32, 1750209

Staff, J. E., Ouyed, R., & Jaikumar, P. 2006, ApJL, 645, L145

Stovall, K., Freire, P. C. C., Antoniadis, J., et al. 2019, ApJ, 870, 74

Sun, X., & Han, J. 2002, Progress in Astronomy, 20, 130

Taam, R. E., & van den Heuvel, E. P. J. 1986, ApJ, 305, 235

Tauris, T. M., & Savonije, G. J. 1999, A&A, 350, 928

Tauris, & van der Klis, M. 2006, Compact Stellar X-ray Sources, eds. W. Lewin & M. van der Klis (Cambridge Univ. Press)

Urpin, V. A., Chanmugam, G., & Sang, Y. 1994, ApJ, 433, 780

Verbunt, F. 1988, Advances in Space Research, 8, 529

Verbunt, F., van den Heuvel, E. P. J., van Paradijs, J., & Rappaport, S. A. 1987, Nature, 329, 312

Wang, B., & Liu, D. 2020, RAA (Research in Astronomy and Astrophysics), 20, 135

Wiktorowicz, G., Drago, A., Pagliara, G., & Popov, S. B. 2017, ApJ, 846, 163

Witten, E. 1984, Phys. Rev. D, 30, 272

Woan, G., Pitkin, M. D., Haskell, B., Jones, D. I., & Lasky, P. D. 2018, ApJL, 863, L40

Xie, Y., & Zhang, S.-N. 2019, ApJ, 880, 123

Xu, R. X. 2003, ApJL, 596, L59

Yoon, S. C., & Langer, N. 2004, A&A, 419, 623

Zahn, J. P. 1977, A&A, 57, 383

Zhang, Y., Geng, J.-J., & Huang, Y.-F. 2018, ApJ, 858, 88

Zhu, C., Lü, G., Wang, Z., & Liu, J. 2013, PASP, 125, 25

Zhu, W. W., Freire, P. C. C., Knispel, B., et al. 2019, ApJ, 881, 165